Published in final edited form as:

*J Neurosurg Pediatr*. ; 24(3): 293–305. doi:10.3171/2019.4.PEDS1994.

# Novel diffusion tractography methodology using Kalman filter prediction to improve preoperative benefit-risk analysis in pediatric epilepsy surgery

**Min-Hee Lee, PhD**[1,5], **Nolan B. O'Hara, MS**[4,5], **Hirotaka Motoi, MD**[1], **Aimee F. Luat, MD**[1,2], **Csaba Juhász, MD, PhD**[1,2,3,4,5], **Sandeep Sood, MD**[3], **Eishi Asano, MD, PhD, MS**[1,2,4], **Jeong-won Jeong, PhD**[1,2,4,5]

[1]Department of Pediatrics, Wayne State University School of Medicine, Detroit

[2]Department of Neurology, Wayne State University School of Medicine, Detroit

[3]Department of Neurosurgery, Wayne State University School of Medicine, Detroit

[4]Department of Translational Neuroscience Program, Wayne State University School of Medicine, Detroit

[5]Translational Imaging Laboratory, Children's Hospital of Michigan, Detroit, Michigan

## Abstract

**Objective—**In this study the authors investigated the clinical reliability of diffusion weighted imaging maximum a posteriori probability (DWI-MAP) analysis with Kalman filter prediction in pediatric epilepsy surgery. This approach can yield a suggested resection margin as a dynamic variable based on preoperative DWI-MAP pathways. The authors sought to determine how well the suggested margin would have maximized occurrence of postoperative seizure freedom (benefit) and minimized occurrence of postoperative neurological deficits (risk).

**Methods—**The study included 77 pediatric patients with drug-resistant focal epilepsy (age 10.0 ± 4.9 years) who underwent resection of their presumed epileptogenic zone. In preoperative DWI tractography from the resected hemisphere, 9 axonal pathways, $C_{i=1-9}$, were identified using DWI-MAP as follows: $C_{1-3}$ supporting face, hand, and leg motor areas; $C_4$ connecting Broca's and Wernicke's areas; $C_{5-8}$ connecting Broca's, Wernicke's, parietal, and premotor areas; and $C_9$ connecting the occipital lobe and lateral geniculate nucleus. For each $C_i$, the resection margin, $d_i$, was measured by the minimal Euclidean distance between the voxels of $C_i$ and the resection boundary determined by spatially coregistered postoperative MRI. If $C_i$ was resected, $d_i$ was assumed to be negative (calculated as –1 × average Euclidean distance between every voxel inside

**Correspondence** Jeong-Won Jeong: Translational Imaging Laboratory, Children's Hospital of Michigan, Wayne State University, Detroit, MI. jjeong@med.wayne.edu.

Author Contributions

Conception and design: Jeong, Asano. Acquisition of data: Jeong, Luat, Sood, Asano. Analysis and interpretation of data: Jeong, Lee, O'Hara, Motoi, Asano. Drafting the article: Jeong, Lee, O'Hara, Juhasz, Sood, Asano. Critically revising the article: Jeong, Luat, Juhasz, Sood, Asano. Reviewed submitted version of manuscript: Jeong, Lee, O'Hara, Motoi, Luat, Juhasz, Asano. Approved the final version of the manuscript on behalf of all authors: Jeong. Statistical analysis: Jeong, Lee, Juhasz. Administrative/technical/material support: Jeong. Study supervision: Jeong.

Disclosures

The authors report no conflict of interest concerning the materials or methods used in this study or the findings specified in this paper.

the resected $C_i$ volume, $r_i$). Kalman filter prediction was then used to estimate an optimal resection margin, $d^*_i$, to balance benefit and risk by approximating the relationship between $d_i$ and $r_i$. Finally, the authors defined the preservation zone of $C_i$ that can balance the probability of benefit and risk by expanding the cortical area of $C_i$ up to $d^*_i$ on the 3D cortical surface.

**Results—**In the whole group (n = 77), nonresection of the preoperative preservation zone (i.e., actual resection margin $d^*_i$ greater than the Kalman filter–defined $d^*_i$ ) accurately predicted the absence of postoperative motor ($d^*_{1–3}$: 0.93 at seizure-free probability of 0.80), language ($d^*_{−4–8}$: 0.91 at seizure-free probability of 0.81), and visual deficits ($d^*_9$: 0.90 at seizure-free probability of 0.75), suggesting that the preservation of preoperative $C_i$ within $d^*_i$ supports a balance between postoperative functional deficit and seizure freedom. The subsequent subgroup analyses found that preservation of preoperative $C_{i=1–4,9}$ within $d^*_{i=1–4,9}$ may provide accurate deficit predictions independent of age and seizure frequency, suggesting that the DWI-based surgical margin can be effective for surgical planning even in young children and across a range of epilepsy severity.

**Conclusions—**Integrating DWI-MAP analysis with Kalman filter prediction may help guide epilepsy surgery by visualizing the margins of the eloquent white matter pathways to be preserved.

### Keywords

diffusion weighted imaging; DWI; tractography; outcome prediction; eloquent areas; functional brain mapping; epilepsy

---

When appropriate pharmaceutical treatment fails to control seizures, children with drug-resistant focal epilepsy should be referred for presurgical evaluation. Early surgical intervention is critical, because persistent seizures can have a negative impact on the developing brain.[9] The major goal of epilepsy surgery is to maximize the chance of postoperative freedom from seizures (benefit) while minimizing postoperative neurological deficits (risk) in sensorimotor, language, and/or visual domains.

Prevention of postoperative deficits requires accurate preoperative mapping of functionally important areas also known as eloquent areas (Xu H, Dong M, Nakai Y, Asano E, Jeong JW: Automatic detection of eloquent axonal pathways in diffusion tractography using intracranial electrical stimulation mapping and convolutional neural networks, presented at the IEEE 15th International Symposium on Biomedical Imaging, Washington, DC, April 4–7, 2018). In many epilepsy centers, invasive electrocorticography (ECoG) recordings and electrical stimulation mapping (ESM) via intracranial electrodes are used to localize the epileptogenic zone and eloquent areas.[16,25] Although such invasive approaches are treated as the current gold standard, ESM does not always have sufficient sensitivity to localize eloquent areas in children at an individual patient level.[18,33] Thus, a more structured and quantitative tool, which is preferably noninvasive, is required to provide an optimal resection margin, taking into account each procedure's potential benefit and risk.

Diffusion weighted imaging (DWI) tractography is a noninvasive technique to visualize white matter pathways,[15] and it has been used in preoperative planning to help in localizing eloquent areas for which resection results in functional deficits.[8,20,35,39] Our previous study[24] of 40 patients suggested that preoperative DWI enables spatial characterization of eloquent pathways in children with focal epilepsy and prediction of the optimal volume of these pathways to preserve, thus minimizing postoperative deficits. In this analysis we applied Bayesian estimations of maximum a posteriori probability to DWI tractography (DWI-MAP) grouped using the QuickBundles algorithm[11,12] to classify eloquent pathways and predict the optimal preserved volume of these pathways to preserve function. The preservation of preoperative eloquent pathways at up to 97% of their volume (i.e., 3% resection) predicted that 88%, 85%, 93%, 99%, and 93% of patients will be without postsurgical deficit in face sensorimotor, hand sensorimotor, leg sensorimotor, language, and visual function, respectively.[24] However, our previous approach was limited to consideration of preoperative pathway volume loss and prevention of postoperative deficit, and we did not consider how well the preservation of an individual pathway achieves the main surgical benefit: seizure freedom.

The goal of the present study was therefore to further expand on and contextualize the clinical utility of improved DWI-MAP analysis in a large cohort of patients (n = 77). The primary methodological improvement is the addition of an integrated Kalman filter,[21] which can preoperatively predict an optimal resection margin to balance benefit and risk by modeling a hidden-state function of the resected DWI-MAP–determined white matter pathways; this information can then be used to predict the surgical outcome in any given patient, including both the presence of postoperative functional deficits and the achievement of seizure freedom. For a given DWI-MAP pathway, the resection margin was clinically determined based on the assessment of ECoG recordings.[2] This actual margin was then analyzed with both the resected volume fraction of DWI-MAP–defined pathways and the surgical outcome via the Kalman filter process, which enabled us to determine the hidden relationship of the resection margin with the observed postoperative outcome and the resected fraction of the preoperative DWI-MAP pathway volume and allowed us to predict an optimal margin to minimize risk while maximizing benefit. The accuracy of this suggested margin was systematically validated in subgroup analyses including patient groups of various ages and seizure frequencies.

# Methods

## Patients

We initially studied 84 patients with drug-resistant focal epilepsy (age 10.0 ± 4.9 years, 42 boys, recruited between 2011 and 2018) who underwent resection of their presumed epileptogenic zone at the Children's Hospital of Michigan (Detroit, MI, USA). None of the included patients had hemiplegia, aphasia, or hemianopsia on examination prior to surgery. All study patients underwent two-stage epilepsy surgery with extraoperative ECoG recording using subdural grid and strip electrodes; the margin of cortical resection was clinically determined based on the locations of seizure onset zones on ECoG and cortical lesions on MRI.[2] Data from 40 children (age 9.0 ± 4.9 years, 18 boys; recruited from 2011 to 2016; see patient profiles in Supplemental Table 1) were used as a modeling dataset (n = 40) to define the optimal surgical margins using a DWI tract classification model which integrates DWI-MAP analysis with Kalman filter prediction. It should be noted that these 40 patients were originally reported in our recent work.[24] To test the reliability of the obtained model in an independent cohort, 37 additional children (age 11.1 ± 4.9 years, 20 boys; recruited from 2017 to 2018, see patient profiles in Table 1) were chosen as a validation dataset (n = 37) from the 44 remaining patients, of whom 7 patients (age 11.5 ± 3.4 years, 4 boys) were excluded due to poor quality of their clinical DWI scans (i.e., spatial artifact, echo-planar imaging [EPI] distortion, and small number of diffusion-encoding gradient directions). It should be noted that both modeling and validation datasets were acquired strictly according to the same inclusion and exclusion criteria. Neither age nor sex statistically differed between the two groups, p value = 0.06 (F statistic = 3.66) and p value = 0.43 (chi-square = 0.63), respectively. The validation dataset was analyzed to determine if the optimal margins obtained from the modeling dataset using the Kalman filter prediction were still effective in prediction of postoperative deficits in an independent dataset not included in the modeling process.

The presence or absence of subacute and newly developed postoperative functional deficits, requiring rehabilitation therapy, was determined clinically by a pediatric neurologist (A.F.L.), as well as by physical, occupational, and speech therapists, between 2 and 3 weeks after resective surgery. All clinical team members were blinded to the results of the imaging data analysis. Postoperative deficits were categorized as 1) face sensorimotor deficit, 2) hand sensorimotor deficit, 3) leg sensorimotor deficit, 4) dysphasia, and 5) visual field deficit. Pre- and postoperative examinations included bedside confrontational visual field testing which is commonly performed and documented in patients of all ages by a board-certified pediatric neurologist. Subsets of older patients also underwent a standard perimetry visual field assessment. Postoperative seizure outcome was evaluated using the International League Against Epilepsy (ILAE) classification every 6 months either at clinical visit or by phone interview.[38] ILAE class in Table 1 was determined at least 1 year after surgery.

This observational study was performed in accordance with policies of the Wayne State University Institutional Review Board. Written consent was obtained from each patient’s guardian, or the requirement for informed consent was waived for patients recruited before 2015. All data were obtained as a part of routine clinical management of the patients. Thus, no prospective intervention was performed to obtain the results of the presented DWI-MAP method, thus ensuring that there was no additional direct risk of harm from this study beyond the existing risk of clinical surgery procedures. No recommendation was made by this study to guide the surgical care, since all DWI-MAP analyses were performed retrospectively.

## Data Analysis

DWI was performed using a 3T scanner with 55 isotropic gradient directions and b = 1000 s/mm$^2$. Pre- and postoperative tractography evaluations (time interval 11.7 ± 11.8 months) were performed by our previously described DWI-MAP analysis.[19,21,24] Briefly, whole-brain tractography of the operated hemisphere was obtained by independent component analysis with a ball and stick model[22] and then sorted into 9 eloquent white matter pathways for each hemisphere using stereotaxic white matter probability maps of age-sex matched healthy controls. These pathways consisted of the following somatosensory pathways. $C_{1-3}$: connecting face, hand, and leg somatosensory cortical areas and the internal capsule and language pathways; $C_4$: connecting Broca's and Wernicke's areas; $C_{5,6,8}$: connecting Broca's, Wernicke's, and parietal areas and the premotor area; $C_7$: connecting Wernicke's area, the parietal area, and the central visual pathway; $C_9$: connecting the occipital lobe and the lateral geniculate nucleus. It should be noted that we reconstructed language pathways $C_{4–7}$ only in the dominant (left) hemisphere. A posteriori probability indicating that a given tract belonged to class $C_i$ was calculated by averaging the probability values of $C_i$ over the entire trajectory under equal class prior assumptions of Bayesian inference[13,14] for all 9 pathways. To further reduce false-positive classification, we applied an additional streamline clustering procedure[24] to $C_{i=1–9}$ that utilized average direct-flip distance (ADFD) $\beta_i$ (i.e., the mean distance of equally sampled bidirectional fibers) between each tract and 9 "exemplar" fibers. See examples presented in Supplemental Fig. 1). These exemplar fibers are the calculated centroid streamlines of each $C_i$ in 32 healthy controls (age 12.3 ± 4.8 years, 17 boys) using the QuickBundles algorithm.[11] Streamlines in individual patients were reclassified based on a $C_i$-specific ADFD threshold, $\beta^*_i$, which was optimized such that a pathway's postoperative volume change [$r_i$ = 100 × (volume of preoperative $C_i$ ∩ volume of resected tissue)/volume of preoperative $C_i$] maximized the prediction of postoperative deficits in a binary logistic regression model. To determine this fractional volume of resected tissue in preoperative DWI space, the resected area was first manually segmented in a postoperative DWI b0 image and then registered to preoperative DWI using the symmetric diffeomorphic image normalization algorithm provided through the Advanced Normalization Tools (ANTs) package.[3]

## Determination of Preservation Zone Balancing Benefit and Risk

During preoperative benefit-risk assessment and determination of resection margin, we needed to calculate the actual distance from a potentially resected epileptic zone to eloquent areas defined by DWI-MAP pathway $C_i$. However, there is no way to estimate a pathway's postoperative volume change, $r_i$, preoperatively, since its estimation requires a postoperative DWI b0 image showing the exact areas that were surgically resected. To overcome this limitation, this study employed Kalman filter prediction, which can estimate the "unmeasurable" $r_i$ from the measurable $d_i$ (i.e., the actual margin of the surgery that was, or will be, done). To test the feasibility of this prediction in the modeling set where the actual measurements $r_i$ and $d_i$ were available from pre- and postoperative DWI data of 40 children with focal epilepsy, we first determined resection margin $d_i$ by coregistering postoperative to preoperative b0 images and calculating the minimal Euclidean distance between voxels of $C_i$ and the surgical resection boundary. In cases where $C_i$ was resected, $d_i$ was assumed to be negative and calculated as −1 × average Euclidean distance between every voxel inside the resected $C_i$ (Fig. 1). The proposed Kalman filter[21] is known as a linear quadratic prediction model and uses a series of two observed variables to identify an unknown relationship (i.e., state) between two variables. Once a significant relationship is identified, we can infer that one variable can accurately predict another variable. In this study, the Kalman filter prediction was modified to approximate the hidden linear-quadratic relationship, $x(r_i)$, between two observation variables, $d_i$ and $r_i$. That is, for a given ith patient, $r_i$ was assumed as a dynamic variable to control the unknown state variable $x(r_i)$ associated with the surgical margin $d_i$. The state variable of the i + 1th patient is then formulated as a function of the state variable, $x(r_i)$ and the measured $r_i$ of the ith patient as follows:

$$x(r_{i+1}) = S_x \times x(r_i) + S_r \times (r_i) + w(r_i),$$

$$d_i = S_d \times x(r_i) + v(r_i),$$

$$w \sim N(0, C_s), \quad x(1) \sim N[x(1), v(1)], \; v \sim N(0, C_d),$$

where the system matrix ($S_x$, $S_r$, $S_d$) is iteratively updated to determine the hidden stochastic process between dynamics [$x(r_i)$] and observation ($d_i$ and $r_i$). $C_s$ and $C_d$ represent system covariance and observation covariance, respectively. $N(\mu, \Sigma)$ indicates white Gaussian noise with mean μ and covariance Σ. The detailed block diagram of the above Kalman filter prediction is presented in Supplemental Fig. 1.

To improve the accuracy of prediction within the small sample size, a fixed-interval smoothing algorithm[28] was used to smooth the Kalman filter–determined $d_i$, $d_i(r_i)$, according to the magnitude of its covariance. Finally, an optimal margin $d^*_i$, balancing seizure freedom with the occurrence of a particular deficit after surgery, was found at $d_i(r_i)$, satisfying P[deficit|$d_i(r_i)$] = P[seizure freedom|$d_i(r_i)$], where P[deficit|$d_i(r_i)$] and P[seizure freedom|$d_i(r_i)$] represent cumulative probability density functions of seizure freedom and deficit, respectively, at $d \leq d_i(r_i)$. Finally, we defined the preservation zone of $C_i$ that balances risk: P[deficit|$d_i(r_i)$], and benefit: P[seizure freedom|$d_i(r_i)$], by expanding the cortical area of $C_i$ (i.e., the cortical terminal) up to the Kalman filter–defined margin, $d^*_i$, on the 3D cortical surface.

## Statistical Analysis

Fisher's exact probability test[1] combined with binary logistic regression analysis was applied to investigate the clinical feasibility of preservation zone of $C_i$ (i.e., preserved/resected) to successfully predict the occurrence of postsurgical functional deficit (i.e., yes/no). Accuracy of this test was evaluated as the proportion of correct predictions [(true positive + true negative)/total number of patients in the study], taken from a 2 × 2 confusion matrix[40] predicting the occurrence of postoperative deficits depending on either preserved or resected $C_i$. To further investigate association between the obtained accuracy and age at MRI or frequency of seizures, we used Spearman's rank correlation for subgroup analyses.

Altogether, the above data-processing pipeline for a prospective patient takes about 30 minutes to obtain the DWI-proposed preservation zones of $C_{i=1-9}$ satisfying $d^*_{1-9}$. This timeframe considers a single patient's preoperative DWI study processed using in-house software implementation combining MATLAB (R2017a; www.mathworks.com) and Python 3.6 (www.python.org) on a graphical processing unit (NVidia GeForce GTX 1080 Ti).

## Results

Across all patients, the following deficits were noted postoperatively for the modeling dataset and the validation dataset, respectively, face sensorimotor deficit (n = 7, 17.5% for modeling dataset; n = 6, 16.2% for validation dataset), hand sensorimotor deficit (n = 6, 15%; n = 7, 18.9%), leg sensorimotor deficit (n = 6, 15%; n = 4, 10.8%), dysphasia (n = 6, including 4 right-sided surgeries and 2 left-sided surgeries, 15%; n = 7, including 7 left-sided surgeries, 18.9%), and visual field deficit (n = 13, 33%; n = 7, 18.9%).

In the modeling dataset (n = 40), binary logistic regression analysis revealed that postoperative fiber loss $r_{1–9}$ of the DWI-MAP–determined pathways $C_{1–9}$ could predict postoperative deficits with high accuracy, resulting in the values 0.93, 1.00, 0.98, 0.98, 0.83, 0.88, 0.85, 0.85, and 0.90 when predicting postoperative deficits in face sensorimotor function ($\beta^*_1$ = 13 mm), hand sensorimotor function, ($\beta^*_2$ = 9 mm), leg sensorimotor function ($\beta^*_3$ = 8 mm), language function ($\beta^*_4$ = 12 mm, $\beta^*_5$ = 13 mm, $\beta^*_6$ = 15 mm, $\beta^*_7$ = 13 mm, $\beta^*_8$ = 17 mm) and visual function ($\beta^*_9$ = 9 mm), respectively. The ADFD thresholds $\beta_{i=1–9}$ for each class $C_i$ were optimized by maximizing the predictive accuracy of postoperative deficits given postoperative fiber loss, $r_{1–9}$. The subsequent Kalman filter analysis also revealed hidden nonlinear state relationships between $r_{1–9}$ and $d_{1–9}$ (Fig. 2), yielding $d^*_{1–9}$ = −1.9, 2.3, −4.8, 1.4, 1.6, 0.7, −2.8, 0.7, and −4.6 mm, which ultimately balanced the values of $P[\text{deficit}|d_i(r_i)]$ and $P[\text{seizure freedom}|d_i(r_i)]$ as plotted on Fig. 3.

To demonstrate the clinical reliability of the preservation zone determined by the preoperative DWI-MAP pathway $C_i$ and the Kalman filter–defined margin $d^*_i$ in patients of the validation dataset, Fig. 4 presents representative examples of surgical resections (patients 7, 9, and 23) that preserved the DWI-proposed preservation zones of the preoperative pathways $C_1$ (face), $C_2$ (hand), $C_3$ (leg), $C_4$ (Broca-Wernicke areas), $C_7$ (Wernicke-parietal areas), and $C_9$ (occipital lobe and lateral geniculate nucleus). None of the patients whose preoperative data are presented in Fig. 4 showed a postoperative deficit related to a given eloquent pathway. On the other hand, Fig. 5 presents representative examples of the preoperative DWI preservation zones (patients 23 and 26) that were surgically resected, as indicated by white arrows. Children whose data are presented in Fig. 5 did show a postoperative deficit related to a given pathway affected by resection. Taken together, these results suggest that the proposed approach may effectively guide surgery and prevent postoperative deficits if the preoperative DWI preservation zones of eloquent pathways are not resected.

Table 2 (modeling dataset, n = 40) and Table 3 (validation dataset, n = 37) show that the actual resection margin $d_i$, when greater than the DWI-proposed surgical margin $d^*_i$ (i.e., when the proposed preservation zone of $C_i$ is preserved or minimally resected within $d^*_i$), achieved high accuracy for predicting functional and seizure outcomes. Accuracy values for a deficit-free outcome with (or without) seizure freedom were measured in the range of 0.75–0.96 (0.81–1.00) for $d^*_{1–9}$. In the combined dataset (n = 40), accuracy values were in the range of 0.83–0.98 to predict postoperative deficit, and 0.67–0.88 to predict postoperative seizure freedom for $d^*_{1–9}$.

Similar (or slightly higher) accuracy values were achieved for the validation dataset (n = 37): 0.91–0.96 (0.86–1.00) for $d^*_{1-9}$, respectively. In the combined dataset (n = 37), accuracy values were in the range of 0.89–0.97 to predict postoperative deficit and 0.78–0.91 to predict postoperative seizure freedom for $d^*_{1-9}$, suggesting high reproducibility of the proposed Kalman filter analysis to predict postoperative outcomes using the DWI-based margin $d^*_{1-9}$.

In whole-group analysis (n = 77), the proposed surgical margin $d^*_{i=1-3}$ predicted somatosensory deficits with a high average accuracy of 0.93 and seizure freedom with an average probability of 0.80. Also, the proposed surgical margin $d^*_{i=4-8}$ predicted language deficits with a high average accuracy of 0.91 and seizure freedom with an average probability of 0.81, and the proposed $d^*_9$ predicted visual deficits with a high average accuracy of 0.90 and seizure freedom with an average probability of 0.75.

Interestingly, subsequent subgroup analyses suggested that the proposed d* provided similar accuracy values for predicting postoperative deficits across the range of patient ages at the time of MRI: 0.74/0.94/0.95/0.94/0.85 for average $d^*_{1-4,9}$ in the whole group (n = 77) for patients ≤ 5 years old (n = 19), 1.00/1.00/1.00/1.00/0.92 for average $d^*_{1-4,9}$ in patients 6–10 years old (n = 17), and 0.87/0.95/0.93/0.92/0.89 for average $d^*_{1-4,9}$ in patients > 10 years old (n = 41). That is, there was no association between accuracy values and age at the MRI (i.e., Spearman's rank coefficient ρ = 0.52/−0.21/−0.03/−0.21/0.35 and p value = 0.30/0.73/1.00/0.73/0.51 for $d^*_{1-4,9}$). This finding offers preliminary evidence that our proposed surgical margin analysis can be successfully applied to young children (i.e., age ≤ 5 years) undergoing presurgical workup. For different frequencies of seizures, high accuracies for prediction of postoperative deficit were achieved with average $d^*_{1-4,9}$ of 0.86/0.96/0.91/0.93/0.87 for the whole group (n = 77) in patients with daily seizures (n = 33), average $d^*_{1-4,9}$ of 0.82/1.00/1.00/0.82/0.89 in patients with weekly seizures (n = 13), and average $d^*_{1-4,9}$ of 0.97/0.91/0.97/1.00/0.91 in patients with monthly seizures (n = 25). There was also no association between accuracy values and frequency of seizures (ρ = −0.54/0.21/−0.52/−0.52/−0.20 and p value = 0.30/0.73/0.33/0.30/0.71 for $d^*_{1-4,9}$). These results further suggest that the preservation of $d^*_i$ may satisfactorily assess the risk of postoperative deficit across a range of epilepsy severity.

## Discussion

The present study provides two major findings. First, a DWI tract classification model integrating DWI-MAP, ADFD, and Kalman filter[21] analysis can define optimal preservation zones of eloquent white matter pathways in patients undergoing resective epilepsy surgery, ultimately helping balance the benefit of seizure freedom with the risk of functional deficit. This analysis considers the potential deficits associated with 9 eloquent white matter pathways, each of which supports sensorimotor, language, or visual function. The DWI-proposed surgical margin around the pathways supporting sensorimotor function ($d^*_{1-3}$) predicted whether the chosen surgical margin would result in a deficit with a high average accuracy of 0.93 and predicted seizure freedom with an average probability of 0.80 in both the modeling and validation datasets. The DWI-defined surgical margins around pathways supporting language function ($d^*_{4-8}$) also predicted postoperative language deficit and seizure freedom with high accuracy (0.91 and 0.81) in the modeling and validation datasets, and the DWI-proposed margin around pathways supporting visual function $d^*_9$ predicted postoperative visual deficit and seizure freedom with high accuracy (0.90 and 0.75) in both modeling and validation datasets. This finding suggests that DWI-based mapping can supplement ESM-derived knowledge by providing a quantitative surgical margin for preserving eloquent tissue at high seizure-free probability. Secondly, the subgroup analyses found that the preservation of the DWI-defined surgical margins $d^*_{i=1–4,9}$ may provide accurate deficit predictions independent of age and seizure frequency. This finding suggests that the DWI-proposed surgical margin can be an effective tool for surgical planning even in young children, for whom cognitive functions are difficult to localize using ESM or functional MRI.

The present study has demonstrated the utility of our proposed surgical margin to minimize functional deficits while maximizing seizure freedom in children with epilepsy. Preoperative planning for these surgeries currently requires multimodal imaging data and multidisciplinary clinician teams.[26] The gold standard information utilized by these teams to determine surgical resection margins primarily comes from implanted intracranial electrodes that record epileptiform discharges and ESM to localize functional cortex.[4–6,30,34] Yet, there are no universally accepted guidelines for how to determine the exact resection margin, or how to integrate multimodal information sources that can supplement each other. Moreover, there is a need to improve approaches to determine surgical margins in a noninvasive manner.

Failure to identify eloquent cortex in proposed resection areas can have potentially lifelong consequences, and overestimating the extent of eloquent areas or incorrectly classifying eloquent areas may lead to incomplete resection of the epileptogenic zone.[17] In fact, the minimum acceptable distance between ESM-identified positive sites and the resection margin is highly variable across different settings, ranging from 0 to 2 cm in survey responses obtained from 56 epilepsy surgery centers.[17] Moreover, approximately 40% of centers reported cases of persistent postoperative language deficit despite preservation of all ESM-identified positive sites.[17] ESM may be supplemented by ECoG-based language mapping, when areas of brain tissue cannot be reliably probed by ESM but still appear to support eloquent function in relevant contexts, and therefore ought to guide resection during surgery.[23,30] Nevertheless, ECoG techniques of identifying eloquent cortex rely on the same implanted subdural electrodes that ESM techniques do, and therefore suffer from many of the same limitations: 1) they are highly invasive techniques and therefore should be applied conservatively, sampling limited regions of the brain; 2) they provide inherently limited information about the brain surface they do sample, because implanted electrodes cannot provide spatially continuous data across their underlying area of cortex.[23,32] In contrast to these modalities, the present study can suggest a quantifiable surgical margin that aims to avoid eloquent white matter pathways defined by preoperative DWI analysis. In addition, our findings suggest that postoperative functional outcome may substantially depend on the extent of resection of preoperative eloquent white matter pathways determined by preoperative DWI-MAP analysis. Our findings are applicable to young children whose ESM and functional MRI studies often fail to detect eloquent areas of interest.[18,31] Therefore, we believe that a sophisticated DWI tractography analysis, utilized as a noninvasive supplemental assessment modality, can provide helpful insights for identifying eloquent areas and minimizing the surgical resection of eloquent areas. In fact, our hierarchical regression analysis (Supplemental Fig. 3) found that the addition of Kalman filtering determined preservation zones ($d^*_{1–4,9}$) to resections of ECoG-based epileptic regions in 4 different lobes provided a significant increment of the correlation coefficient, $R^2$, to predict postoperative deficits of 160% (visual deficit), 180% (face deficit), 340% (hand deficit), 470% (leg deficit), and 510% (language deficit). This observation infers that the proposed methodology based on DWI tractography provides an additional value to predict postoperative deficits before surgery (i.e, especially for language function).

There are several limitations that need to be considered in the present study. First, all data were obtained for the clinical management of epilepsy surgery. Therefore, these are retrospective and observational results with inherent limitations to the sample size and information on the severity of postoperative deficits due to restricted availability of detailed functional testing measures. Further prospective studies are needed in larger numbers of children, with availability of detailed information regarding postoperative deficits, especially in young children. Second, the present study focused on subacute postoperative deficits. Therefore, assessment of the relationship between surgical margins and long-term changes in postoperative deficits, or of the responsiveness of these deficits to physical or cognitive therapies, is beyond the scope of this study. Further comparative studies are warranted to investigate how well the proposed methodology can predict the severity of permanent postoperative deficits. Third, it remains unclear whether DWI tractography is capable of accurately deriving long-range anatomical connections,[29,36] especially in cases with severe white matter loss often accompanied by developmental delay, tumor, and cortical tubers. Limited scan time restricts the number of diffusion-encoding directions for imaging cortical terminals of eloquent pathways at a relatively low diffusion weight (i.e., b = 1000 s/$mm^2$). Considering these inherent challenges of DWI tractography, only shorter-range motor pathways connecting the primary motor cortex and the posterior limb of the internal capsule, as well as major pathways of language and vision, which are anatomically consistent with postmortem human brain studies,[10,37] were considered in the present study. Therefore, the DWI-proposed surgical margins are limited to the consideration of these 9 eloquent white matter pathways. The logical next step is to validate our method prospectively in a larger cohort of patients who undergo resective epilepsy surgery.

## Supplementary Material

Refer to Web version on PubMed Central for supplementary material.

## Acknowledgements

The authors would like to thank all participants and their families for their time and interest in this study. We also appreciate Mrs. Alanna Marie Carlson and Dr. Robert Rothermel for clinical neuropsychological assessment. This study was funded by grants from the National Institutes of Health (R01 NS089659 to J.W.J. and R01 NS064033 to E.A.).

## Abbreviations

| | |
|---|---|
| **ADFD** | average direct-flip distance |

| | |
|---|---|
| **DWI** | diffusion weighted imaging |
| **DWI-MAP** | DWI maximum a posteriori probability |
| **ECoG** | electrocorticography |
| **ESM** | electrical stimulation mapping |
| **ILAE** | International League Against Epilepsy |

## References:

1. Agresti A: A survey of exact inference for contingency tables. Statist Sci 7:131–153, 1992
2. Asano E, Juhász C, Shah A, Sood S, Chugani HT: Role of subdural electrocorticography in prediction of long-term seizure outcome in epilepsy surgery. Brain 132:1038–1047, 2009 [PubMed: 19286694]
3. Avants B, Gee JC: Geodesic estimation for large deformation anatomical shape averaging and interpolation. Neuroimage 23:S139–S150, 2004 [PubMed: 15501083]
4. Bauer PR, Vansteensel MJ, Bleichner MG, Hermes D, Ferrier CH, Aarnoutse EJ, et al. : Mismatch between electrocortical stimulation and electrocorticography frequency mapping of language. Brain Stimul 6:524–531, 2013 [PubMed: 23395595]
5. Borchers S, Himmelbach M, Logothetis N, Karnath HO: Direct electrical stimulation of human cortex - the gold standard for mapping brain functions? Nat Rev Neurosci 13:63–70, 2011 [PubMed: 22127300]
6. Cho JH, Kang HC, Jung YJ, Lee YH, Jung KY, Kim HD, et al. : Localization of ictal onset zones in Lennox–Gastaut syndrome (LGS) based on information theoretical time delay analysis of intracranial electroencephalography (iEEG). Epilepsy Res 99:78–86, 2012 [PubMed: 22071552]
7. Chugani HT, Asano E, Juhász C, Kumar A, Kupsky WJ, Sood S: "Subtotal" hemispherectomy in children with intractable focal epilepsy. Epilepsia 55:1926–1933, 2014 [PubMed: 25366422]
8. Dimou S, Battisti RA, Hermens DF, Lagopoulos J: A systematic review of functional magnetic resonance imaging and diffusion tensor imaging modalities used in presurgical planning of brain tumour resection. Neurosurg Rev 36:205–214, 2013 [PubMed: 23187966]
9. Ducis K, Guan J, Karsy M, Bollo RJ: Preoperative evaluation and surgical decision-making in pediatric epilepsy surgery. Transl Pediatr 5:169–179, 2016 [PubMed: 27709099]
10. Fernández-Miranda JC, Wang Y, Pathak S, Stefaneau L, Verstynen T, Yeh FC: Asymmetry, connectivity, and segmentation of the arcuate fascicle in the human brain. Brain Struct Funct 220:1665–1680, 2015 [PubMed: 24633827]
11. Garyfallidis E, Brett M, Correia MM, Williams GB, Nimmo-Smith I: QuickBundles, a method for tractography simplification. Front Neurosci 6:175, 2012 [PubMed: 23248578]
12. Garyfallidis E, Côté MA, Rheault F, Sidhu J, Hau J, Petit L, et al. : Recognition of white matter bundles using local and global streamline-based registrations and clustering. Neuroimage 170:283–295, 2018 [PubMed: 28712994]
13. Gauvain JL, Lee CH: Maximum a posteriori estimation for multivariate gaussian mixture observations of Markov chains. IEEE Trans Speech Audio Process 2:291–298, 1994
14. Gelman A, Carlin JB, Stern HS, Dunson DB, Vehtari A, Rubin DB: Bayesian data analysis, ed 3: Chapman and Hall/CRC, 2013
15. Guevara P, Duclap D, Poupon C, Marrakchi-Kacem L, Fillard P, Le Bihan D, et al. : Automatic fiber bundle segmentation in massive tractography datasets using a multi-subject bundle atlas. Neuroimage 61:1083–1099, 2012 [PubMed: 22414992]
16. Hader WJ, Tellez-Zenteno J, Metcalfe A, Hernandez-Ronquillo L, Wiebe S, Kwon CS, et al. : Complications of epilepsy surgery: a systematic review of focal surgical resections and invasive EEG monitoring. Epilepsia 54:840–847, 2013 [PubMed: 23551133]

17. Hamberger MJ, Williams AC, Schevon CA: Extraoperative neurostimulation mapping: results from an international survey of epilepsy surgery programs. Epilepsia 55:933–939, 2014 [PubMed: 24816083]
18. Haseeb A, Asano E, Juhász C, Shah A, Sood S, Chugani HT: Young patients with focal seizures may have the primary motor area for the hand in the postcentral gyrus. Epilepsy Res 76:131–139, 2007 [PubMed: 17723289]
19. Jeong JW, Asano E, Brown EC, Tiwari VN, Chugani DC, Chugani HT: Automatic detection of primary motor areas using diffusion MRI tractography: Comparison with functional MRI and electrical stimulation mapping. Epilepsia 54:1381–1390, 2013 [PubMed: 23772829]
20. Jeong JW, Asano E, Juhász C, Chugani HT: Localization of specific language pathways using diffusion-weighted imaging tractography for presurgical planning of children with intractable epilepsy. Epilepsia 56:49–57, 2015 [PubMed: 25489639]
21. Jeong JW, Asano E, Juhász C, Chugani HT: Quantification of primary motor pathways using diffusion MRI tractography and its application to predict postoperative motor deficits in children with focal epilepsy. Hum Brain Mapp 35:3216–3226, 2014 [PubMed: 24142581]
22. Jeong JW, Asano E, Yeh FC, Chugani DC, Chugani HT: Independent component analysis tractography combined with a ball-stick model to isolate intra-voxel crossing fibers of the corticospinal tracts in clinical diffusion MRI. Magn Reson Med 70:441–453, 2013 [PubMed: 23001816]
23. Kuruvilla A, Flink R: Intraoperative electrocorticography in epilepsy surgery: useful or not? Seizure 12:577–584, 2003 [PubMed: 14630497]
24. Lee MH, O'Hara NB, Nakai Y, Luat AF, Juhász C, Sood S, et al. : Prediction of postoperative deficits using an improved diffusion weighted imaging maximum a posteriori probability analysis in pediatric epilepsy surgery. J Neurosurg Pediatr:in press, 2019
25. Lesser RP, Crone NE, Webber WRS: Subdural electrodes. Clin Neurophysiol 121:1376–1392, 2010 [PubMed: 20573543]
26. Nowell M, Rodionov R, Zombori G, Sparks R, Winston G, Kinghorn J, et al. : Utility of 3D multimodality imaging in the implantation of intracranial electrodes in epilepsy. Epilepsia 56:403–413, 2015 [PubMed: 25656379]
27. O'Donnell LJ, Suter Y, Rigolo L, Kahali P, Zhang F, Norton I, et al. : Automated white matter fiber tract identification in patients with brain tumors. NeuroImage Clin 13:138–153, 2017 [PubMed: 27981029]
28. Rauch HE, Tung F, Striebel CT: Maximum likelihood estimates of linear dynamic systems. AIAA J 3:1445–1450, 1965
29. Reveley C, Seth AK, Pierpaoli C, Silva AC, Yu D, Saunders RC, et al. : Superficial whitematter fiber systems impede detection of long-range cortical connections in diffusion MR tractography. Proc Natl Acad Sci U S A 112:E2820–E2828, 2015 [PubMed: 25964365]
30. Ritaccio AL, Brunner P, Schalk G: Electrical stimulation mapping of the brain: Basic principles and emerging alternatives. J Clin Neurophysiol 35:86–97, 2018 [PubMed: 29499015]
31. Roland JL, Griffin N, Hacker CD, Vellimana AK, Akbari SH, Shimony JS, et al. : Resting-state functional magnetic resonance imaging for surgical planning in pediatric patients: a preliminary experience. J Neurosurg Pediatr 20:583–590, 2017 [PubMed: 28960172]
32. Rosenow F, Lüders H: Presurgical evaluation of epilepsy. Brain 124:1683–1700, 2001 [PubMed: 11522572]
33. Schevon CA, Carlson C, Zaroff CM, Weiner HJ, Doyle WK, Miles D, et al. : Pediatric language mapping: sensitivity of neurostimulation and Wada testing in epilepsy surgery. Epilepsia 48:539–545, 2007 [PubMed: 17284300]
34. Smith JL: Chapter 128 - Management of neural tube defects, hydrocephalus, refractory epilepsy, and central nervous system infections., ed 7: Pediatric Surgery, 2012
35. Soni N, Mehrotra A, Behari S, Kumar S, Gupta N: Diffusion-tensor imaging and tractography application in pre-operative planning of intra-axial brain lesions. Cureus 9:e1739, 2017 [PubMed: 29209586]

36. Thomas C, Ye FQ, Irfanoglu MO, Modi P, Saleem KS, Leopold DA, et al. : Anatomical accuracy of brain connections derived from diffusion MRI tractography is inherently limited. Proc Natl Acad Sci U S A 111:16574–16579, 2014 [PubMed: 25368179]
37. Wang X, Pathak S, Stefaneanu L, Yeh FC, Li S, Fernandez-Miranda JC: Subcomponents and connectivity of the superior longitudinal fasciculus in the human brain. Brain Struct Funct 221:2075–2092, 2016 [PubMed: 25782434]
38. Wieser HG, Blume WT, Fish D, Goldensohn E, Hufnagel A, King D, et al. : ILAE Commission Report. Proposal for a new classification of outcome with respect to epileptic seizures following epilepsy surgery. Epilepsia 42:282–286, 2001 [PubMed: 11240604]
39. Winston GP, Yogarajah M, Symms MR, McEvoy AW, Micallef C, Duncan JS: Diffusion tensor imaging tractography to visualize the relationship of the optic radiation to epileptogenic lesions prior to neurosurgery. Epilepsia 52:1430–1438, 2011 [PubMed: 21569018]
40. Zhu W, Zeng N, Wang N: Sensitivity, specificity, accuracy, associated confidence interval and ROC analysis with practical SAS implementations., presented at the Proceedings of NESUG, November 14–17, Baltimore, November 14–17, 2010 (https://www.lexjansen.com/nesug10/hl/hl07.pdf) [Accessed April 29, 2019]

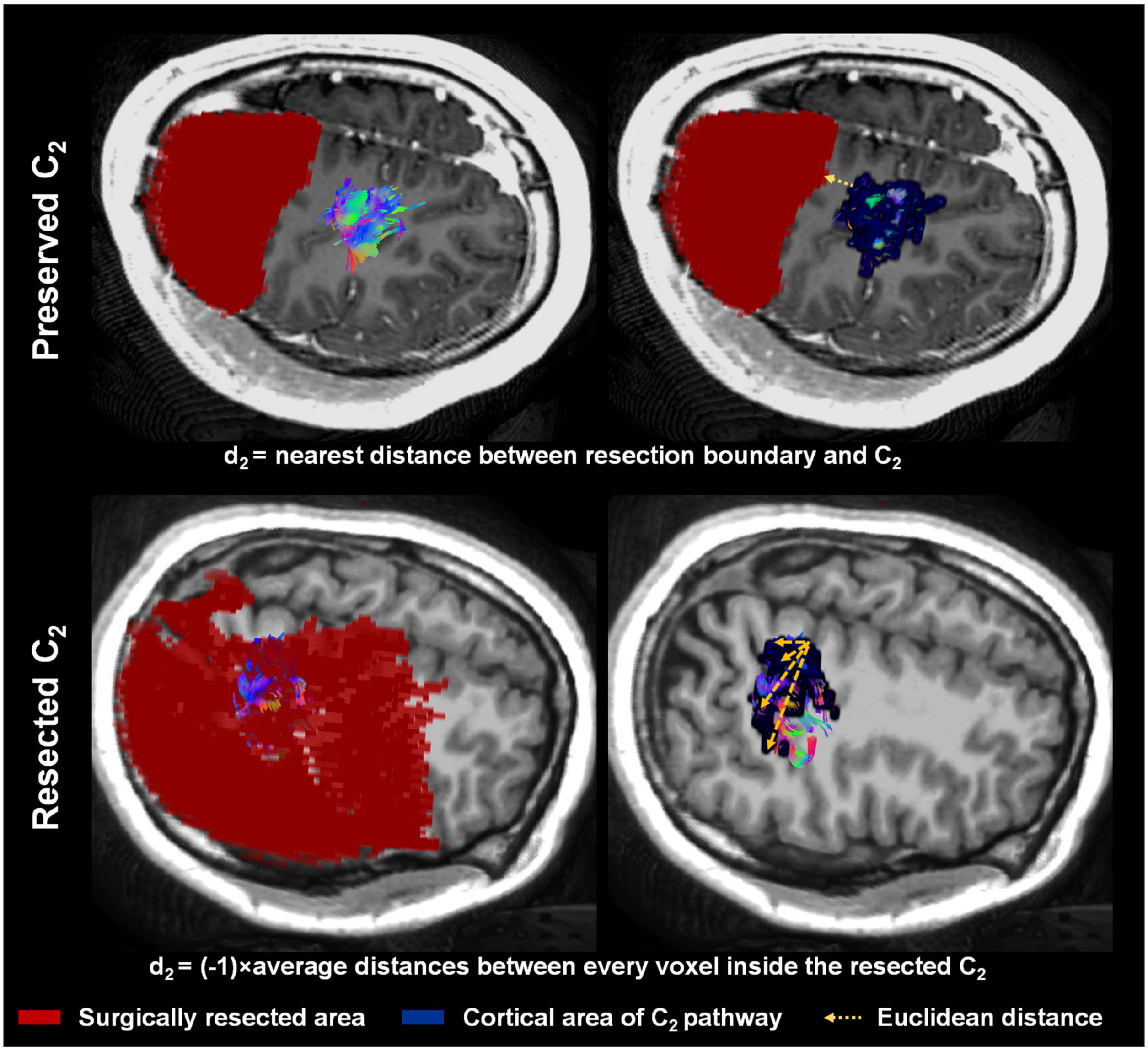


**Figure 1.**

Calculation of actual resection margin $d_{i=2}$ based on its association with $C_{i=2}$. In cases where $C_2$ was preserved, $d_2$ was calculated as the minimal Euclidean distance between the resection boundary and voxels of $C_2$. **Upper:** Patient 22 in the validation set, who showed no postoperative hand weakness. In cases where $C_2$ was affected by resection, $d_2$ was assumed to be negative and calculated as $-1 \times$ average Euclidean distance between every voxel inside the resected $C_2$. **Lower:** Patient 33 in the validation set, who did show postoperative hand weakness.

Author Manuscript
Author Manuscript
Author Manuscript



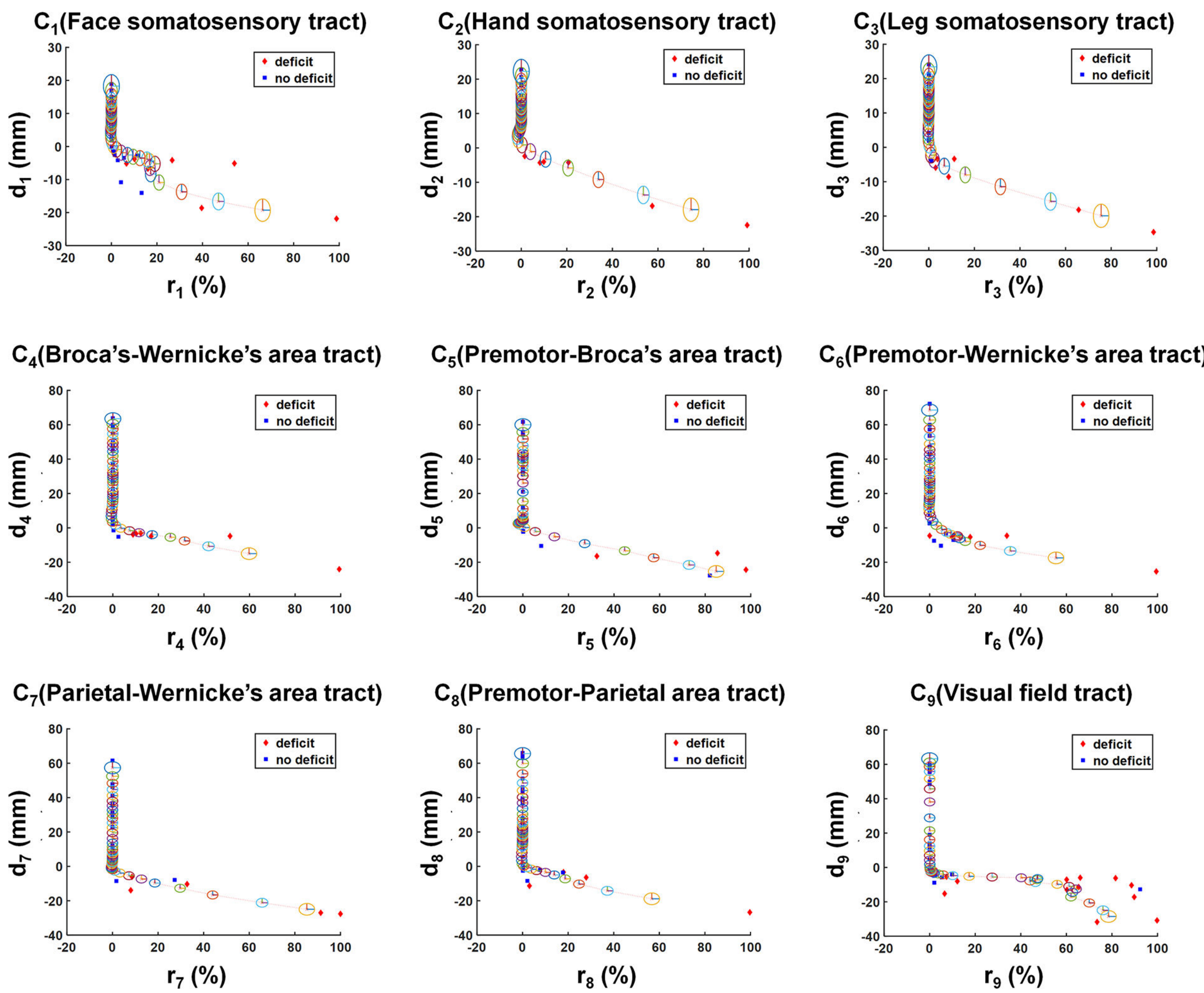


**Figure 2.**

2D plots showing the hidden relationship between resection margin, $d_i$, and postoperative volume changes of $C_i$, $r_i$, which were measured in pre- and postoperative DWI data of the modeling dataset (Supplemental Table 1, n = 40). In each plot, *red diamonds* and *blue squares* indicate patients with and without postoperative deficit, respectively. Kalman filter prediction using the Rauch-Tung-Striebel algorithm[27] was applied to fit $d_i$ as a function of a dynamic variable $r_i$, resulting in $d_i(r_i)$ (*red dotted line*). The radius of each *colored ellipsis* indicates the covariance of the state variable $x(r_i)$, approximating the 95% CI of $d_i(r_i)$.

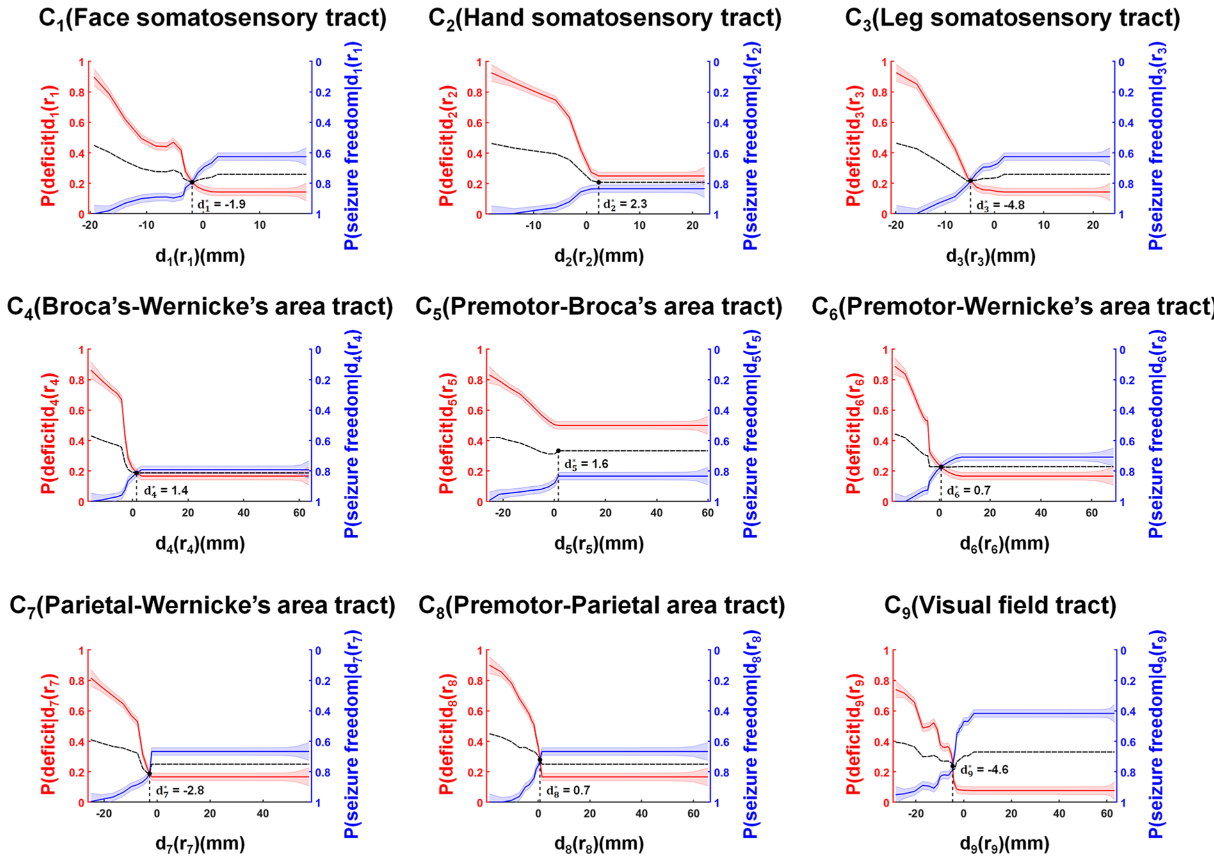


**Figure 3.**

Identification of the proposed margin, $d^*_{i=1-9}$ = −1.9, 2.3, −4.8, 1.4, 1.6, 0.7, −2.8, 0.7, and −4.6 mm, which were optimized to balance P[deficit|$d_{i=1-9}$(r $_{i=1-9}$)] versus P[seizure freedom|$d_{i=1-9}$(r $_{i=1-9}$)] at DWI-MAP–determined $C_{i=1-9}$ of the preoperative DWI data in the modeling dataset (Supplemental Table 1, n = 40). *Solid red and blue lines* indicate the values of the predicted P[deficit|$d_i(r_i)$] and P[seizure freedom|$d_i(r_i)$], where the width of the strips indicates ± 1 × covariance of the predicted P[deficit|$d_i(r_i)$] and P[seizure freedom|$d_i(r_i)$], estimated from covariance of the state variable $x(r_i)$ (Fig. 2). A *dotted black line* indicates the average value of P[deficit|$d_i(r_i)$] and P[seizure freedom|$d_i(r_i)$], balancing both risk and benefit as a function of $d_i(r_i)$.

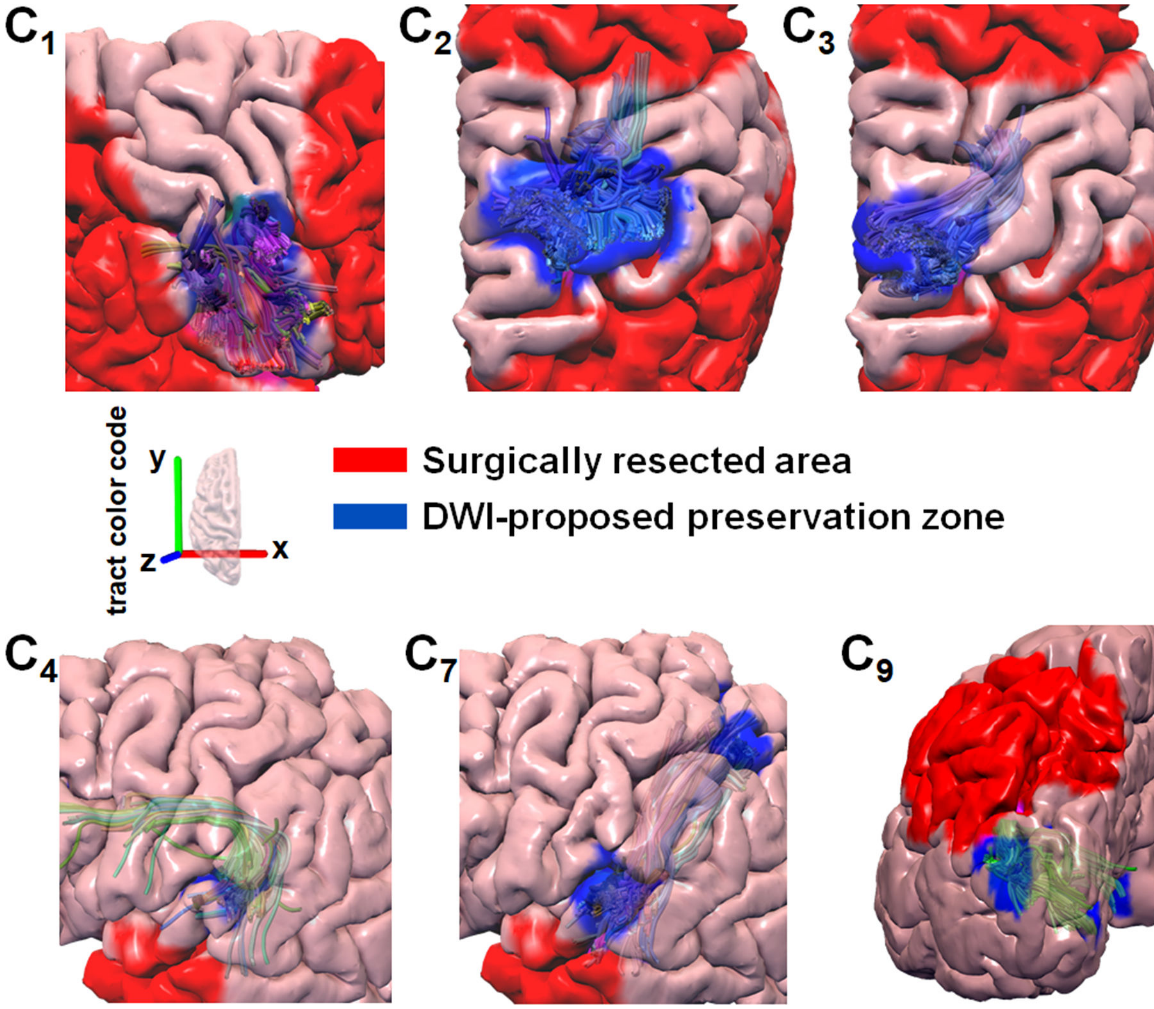


**Figure 4.**

Representative examples of surgical resections (*red area*) that preserved the DWI-proposed preservation zone determined by the preoperative DWI-MAP pathway $C_i$ and Kalman filter–defined margin $d^*_i$ (*blue area*). Preoperative tract pathways $C_1$ (face sensorimotor), $C_2$ (hand sensorimotor), and $C_3$ (leg sensorimotor) were obtained from patient 23 in the validation set, who had no postoperative face, hand, or leg deficits. Preoperative tract pathways $C_4$ (Broca-Wernicke areas) and $C_7$ (Wernicke-parietal areas) were obtained from patient 7 in the validation set who had no postoperative language deficits. Preoperative tract pathway $C_9$ (occipital lobe and the lateral geniculate nucleus) was obtained from patient 9 in the validation set, who had no postoperative visual field deficits. It is clear that none of the patients whose DWI-proposed preservation zones of preoperative pathways were preserved showed a postoperative deficit related to a given eloquent pathway.

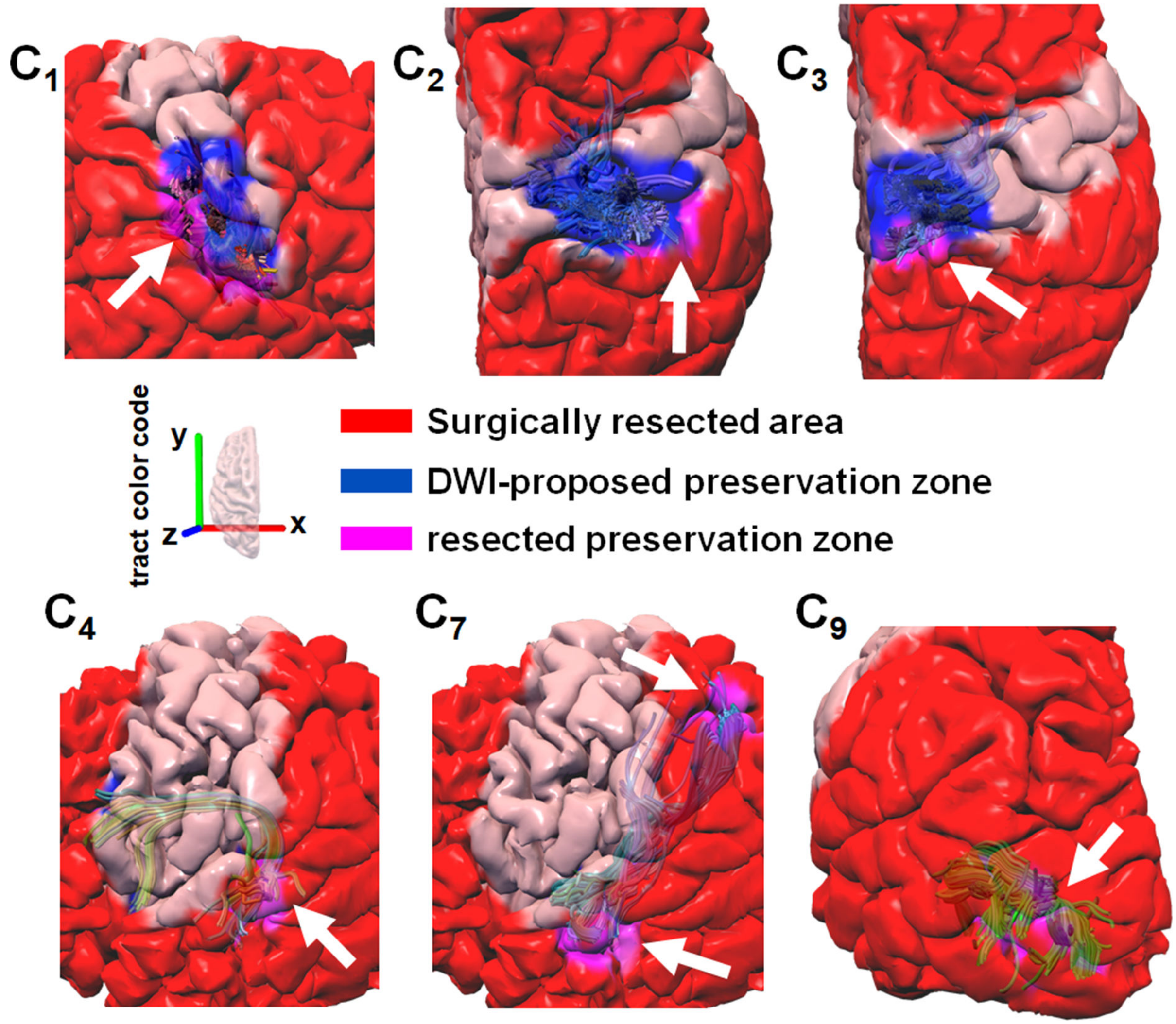


**Figure 5.**

Representative examples of surgical resections (*red area*) including some portion (*magenta area*) of the DWI-proposed preservation zone determined by the preoperative DWI-MAP pathway $C_i$ and Kalman filter–defined margin $d^*_i$ (*blue area*). Preoperative tract pathways $C_1$ (face sensorimotor), $C_2$ (hand sensorimotor), and $C_3$ (leg sensorimotor) shown for patient 26 in the validation set, who had postoperative face, hand, and leg weakness. Preoperative tract pathways $C_4$ (Broca-Wernicke areas) and $C_7$ (Wernicke-parietal areas) are shown for patient 23 in the validation set, who had a postoperative language deficit, and $C_9$ (occipital lobe–lateral geniculate nucleus) are shown for patient 23 in the validation set, who had postoperative visual field deficits. *White arrows* highlight where the proposed margin $d^*_i$ was affected by resective surgery, which may cause postoperative deficit related to a given pathway.

**Table 1.**

Clinical variables of the study subjects in validation dataset (n= 37).

| No | Age | Gender | Side | Resection lobe | Postoperative deficit | ILAE class | Seizure frequency |
|---|---|---|---|---|---|---|---|
| 1 | 10 | B | Lt | T | No | 1 | 2–3/week |
| 2 | 10 | G | Rt | T | No | 3 | 1–2/month |
| 3 | 11 | G | Rt | P | H,L | 1 | 10/day |
| 4 | 5 | B | Lt | F | Lg | 1 | 15–20/day |
| 5 | 14 | G | Rt | T,P,O | No | 5 | 3–4/week |
| 6 | 16 | B | Lt | T,O | No | 4 | 1–2/month |
| 7 | 9 | G | Lt | T | No | 1 | Unknown |
| 8 | 6 | G | Lt | T | No | 1 | 1/month |
| 9 | 12 | G | Lt | P | No | 1 | 1/month |
| 10 | 16 | B | Rt | F | Fa | 1 | 2–3/month |
| 11 | 17 | B | Rt | T | No | 1 | 1/month |
| 12 | 12 | B | Rt | T | No | 1 | 1/day |
| 13 | 12 | G | Rt | F | No | 1 | 1–2/month |
| 14 | 14 | B | Rt | T,P,O | No | 1 | 1–2/month |
| 15 | 9 | B | Rt | F,T,P,O | Fa,H | 3 | 4/day |
| 16 | 14 | G | Rt | T | V | 1 | 2–3/month |
| 17 | 16 | B | Rt | T | No | 1 | 0.5/year |
| 18 | 14 | G | Rt | T | No | 1 | 1–2/month |
| 19 | 18 | B | Rt | F,P | V | 4 | 1/day |
| 20 | 12 | B | Rt | T,P | H,L,V | 1 | 1–2/day |
| 21 | 12 | B | Lt | T | No | 3 | 1–2/month |
| 22 | 13 | G | Lt | F | Lg | 5 | 2–3/week |
| 23 | 3 | G | Lt | F,T,P,O | Lg,V | 5 | 2–6/day |
| 24 | 5 | B | Rt | T | No | 1 | 3–4/month |
| 25 | 3 | B | Lt | T,P,O | Lg,V | 1 | Unknown |
| 26 | 2 | B | Rt | F,T,P,O | Fa,H,L | 1 | 2–3/day |
| 27 | 2 | B | Rt | P | No | 1 | Unknown |
| 28 | 13 | B | Lt | T | No | 4 | 3/week |
| 29 | 6 | G | Lt | P,O | Fa,H,Lg | 4 | 1–2/month |
| 30 | 11 | B | Rt | T | No | 1 | 1–3/month |
| 31 | 5 | B | Lt | F | Fa,H,Lg | 1 | 20–30/day |
| 32 | 5 | G | Lt | T,P,O | Lg,V | 1 | 1/day |
| 33 | 16 | G | Rt | P | Fa,H,L | 3 | 1–2/month |
| 34 | 18 | G | Lt | O | No | 1 | 5–10/day |
| 35 | 17 | B | Rt | T | No | 3 | 2–3/month |
| 36 | 14 | G | Lt | T | V | 3 | 5/month |
| 37 | 18 | G | Rt | P | No | 2 | 11/day |

Age: years old at preoperative MRI, G/B: girl/boy, Lt/Rt: left/right, F/T/P/O: frontal/temporal/parietal/occipital, FTPO resection is consistent with subtotal hemispherectomy[41]. Fa/H/L/Lg/V: face/hand/leg/language/visual.

**Table 2.**

Accuracy of the proposed surgical margin to predict postoperative deficit in face weakness ($d_1^* = -1.9$ mm), hand weakness ($d_2^* = 2.3$ mm), leg weakness ($d_3^* = -4.8$ mm), language ($d_{4-8}^* = 1.4, 1.6, 0.7, -2.8$ mm) and visual field ($d_9^* = -4.6$ mm) in the modeling dataset (Supplemental Table 1, n=40). Values are listed for eleven different modeling groups/subgroups: seizure free (n=24), not seizure free (n=16), combined set (n=40), age at MRI ≤ 5 years old (n=11), age at MRI 6–10 years old (n=11), age at MRI > 10 years old (n=18), daily seizures (n=21), weekly seizures (n=9) and monthly seizures (n=8). [ ] indicates the probability of seizure freedom while preserving $d^*$ (i.e., $d > d^*$ in mm): $P(seizure\ freedom|d_i^*)$.

| Group (n) | $d_1^*$ | $d_2^*$ | $d_3^*$ | $d_4^*$ | $d_5^*$ | $d_6^*$ | $d_7^*$ | $d_8^*$ | $d_9^*$ |
|---|---|---|---|---|---|---|---|---|---|
| Seizure free (24) | 0.83 | 0.96 | 0.96 | 0.96 | 0.75 | 0.83 | 0.88 | 0.75 | 0.92 |
| Not seizure free (16) | 0.88 | 1.00 | 0.94 | 0.94 | 0.94 | 1.00 | 0.94 | 0.94 | 0.81 |
| Combined set (40) | 0.85 [0.67] | 0.98 [0.79] | 0.95 [0.88] | 0.95 [0.79] | 0.83 [0.83] | 0.90 [0.67] | 0.90 [0.79] | 0.83 [0.67] | 0.88 [0.67] |
| age at MRI ≤ 5 years old (11) | 0.73 [0.40] | 1.00 [0.40] | 0.91 [0.60] | 1.00 [0.80] | 0.91 [0.60] | 0.91 [0.60] | 1.00 [0.80] | 0.91 [0.60] | 0.82 [0.40] |
| age at MRI 6–10 years old (11) | 1.00 [1.00] | 1.00 [1.00] | 1.00 [1.00] | 1.00 [0.86] | 0.73 [0.86] | 1.00 [0.86] | 1.00 [0.86] | 0.82 [0.86] | 1.00 [0.86] |
| age at MRI > 10 years old (18) | 0.83 [0.67] | 0.94 [0.83] | 0.94 [0.92] | 0.89 [0.75] | 0.83 [0.92] | 0.83 [0.58] | 0.78 [0.75] | 0.78 [0.58] | 0.83 [0.58] |
| Daily seizure (21) | 0.81 [0.45] | 1.00 [0.73] | 0.91 [0.82] | 0.95 [0.82] | 0.86 [0.91] | 0.91 [0.73] | 0.95 [1.00] | 0.91 [0.73] | 0.91 0.82] |
| Weekly seizure (9) | 0.89 [1.00] | 1.00 [1.00] | 1.00 [1.00] | 0.89 [0.83] | 0.67 [0.67] | 0.89 [0.67] | 0.89 [0.83] | 0.78 [0.67] | 0.78 [0.67] |
| Monthly seizure (8) | 1.00 [0.80] | 0.88 [0.60] | 1.00 [0.80] | 1.00 [0.80] | 1.00 [0.80] | 0.88 [0.60] | 0.75 [0.40] | 0.88 [0.60] | 0.88 [0.60] |

**Table 3.**

Accuracy of the proposed surgical margin to predict postoperative deficit in face weakness ($d_1^* = -1.9$ mm), hand weakness ($d_2^* = 2.3$ mm), leg weakness ($d_3^* = -4.8$ mm), language ($d_{4-8}^* = 1.4, 1.6, 0.7, -2.8$ mm) and visual field ($d_9^* = -4.6$ mm) in the validation dataset (Table 1, n=37). Values are listed for nine different validation groups/subgroups: seizure free (n=23), not seizure free (n=14), combined set (n=37), age at MRI ≤ 5 years old (n=8), age at MRI 5–10 years old (n=6), age at MRI > 10 years old (n=23), daily seizures (n=12), weekly seizures (n=4) and monthly seizures (n=17). [ ] indicates the observed probability of seizure freedom while preserving $d^*$ (i.e., $d > d^*$ in mm): $P(\textit{seizure freedom} | d_i^*)$.

| **Group (n)** | $d_1^*$ | $d_2^*$ | $d_3^*$ | $d_4^*$ | $d_5^*$ | $d_6^*$ | $d_7^*$ | $d_8^*$ | $d_9^*$ |
|---|---|---|---|---|---|---|---|---|---|
| Seizure free (23) | 0.91 | 0.96 | 0.96 | 0.96 | 0.91 | 0.91 | 0.96 | 0.96 | 0.91 |
| Not seizure free (14) | 0.86 | 0.93 | 0.93 | 0.93 | 0.93 | 1.00 | 0.86 | 1.00 | 0.93 |
| Combined set (37) | 0.89 [0.78] | 0.95 [0.78] | 0.95 [0.91] | 0.95 [0.87] | 0.92 [0.91] | 0.95 [0.83] | 0.92 [0.87] | 0.97 [0.87] | 0.92 [0.83] |
| age at MRI ≤ 5 years old (8) | 0.75 [0.57] | 0.88 [0.71] | 1.00 [0.86] | 0.88 [0.57] | 0.75 [0.71] | 0.88 [0.57] | 0.88 [0.57] | 0.88 [0.57] | 0.88 [0.57] |
| age at MRI 6–10 years old (6) | 1.00 [1.00] | 1.00 [1.00] | 1.00 [1.00] | 1.00 [1.00] | 0.83 [1.00] | 1.00 [1.00] | 1.00 [1.00] | 1.00 [1.00] | 0.83 [1.00] |
| age at MRI > 10 years old (23) | 0.91 [0.85] | 0.96 [0.77] | 0.91 [0.92] | 0.96 [1.00] | 1.00 [1.00] | 0.96 [0.92] | 0.91 [1.00] | 1.00 [1.00] | 0.96 [0.92] |
| Daily seizure (12) | 0.92 [0.88] | 0.92 [0.50] | 0.92 [0.75] | 0.92 [0.75] | 0.92 [0.75] | 0.92 [0.75] | 0.92 [0.75] | 0.92 [0.75] | 0.83 [0.63] |
| Weekly seizure (4) | 0.75 [1.00] | 1.00 [1.00] | 1.00 [1.00] | 0.75 [1.00] | 1.00 [1.00] | 1.00 [1.00] | 0.5 [1.00] | 1.00 [1.00] | 1.00 [1.00] |
| Monthly seizure (17) | 0.94 [0.80] | 0.94 [0.90] | 0.94 [1.00] | 1.00 [1.00] | 0.94 [1.00] | 0.94 [0.90] | 1.00 [1.00] | 1.00 [1.00] | 0.94 [1.00] |